Available online at www.sciencedirect.com
ScienceDirect
Ceramics International 37 (2011) 791–796
CERAMICS INTERNATIONAL
www.elsevier.com/locate/ceramint

Growth and structural characteristics of perovskite–wurtzite oxide ceramics thin films

Yuan-Chang Liang *

Institute of Materials Engineering, National Taiwan Ocean University, No.2, Peining Rd., Keelung City 20224, Taiwan

Received 7 July 2010; received in revised form 16 August 2010; accepted 8 October 2010
Available online 18 November 2010

Abstract

Wurtzite ZnO thin films were grown on single-crystal perovskite $SrTiO_3$(STO) (1 0 0) substrates at various temperatures. The ZnO/STO thin films thus formed exhibit a preferred (1 1 0)-orientation at a growth temperature of 600–700 °C. A high growth temperature enhances not only the (1 1 0)-texture of ZnO/STO thin films but also the crystalline quality of the film. $(La_{0.7}Sr_{0.3})MnO_3$ (LSMO) thin films were subsequently grown on ZnO(1 1 0)/STO(1 0 0) substrates with various thicknesses, and were polycrystalline. A thicker LSMO film has a stronger (0 0 *l*)-preferred orientation than the thinner one. The lattice distortion of LSMO decreases as the LSMO thickness increases. Magnetization vs. temperature curves show that both crystalline quality and lattice distortion influence the magnetic properties of LSMO thin films. The physical properties of the manganite oxide can be modulated by forming a heterostructure with wurtzite ZnO.

Keywords: A. Films; B. Surfaces; D. Perovskites; D. ZnO

1. Introduction

Of all transition metal oxides, the perovskites (ABO_3-type oxides) have attracted much interest in recent years. Perovskite manganite films are quite stable at room temperature [1]. This feature is critical to the reliability of device applications. Manganese perovskites have the advantage that their transition from a paramagnetic insulator to a ferromagnetic metal can be tuned by controlling the doping rate and the species of di- and trivalent metal ions. Thin films of these materials are considered to have potential for the development of novel electronic devices [2–5]. Recently, the modulation of physical properties of perovskite manganite thin films by incorporating a perovskite oxide, which has a different physical form, into it, to produce a heterostructure is proposed. This modulation of physical properties of a manganite-based heterostructure has been attributed to structural and magnetic modifications at the interface between the two constituent materials [6,7].

ZnO is a wide-bandgap semiconductor with a very large exciton binding energy of 60 meV. It has attracted considerable interest because of its potential applications in optoelectronic devices [8,9]. Manganites have remarkable physical properties and are potential in applications of novel devices, and ZnO has versatile optoelectronic properties. A thin-film heterostructure that comprises these two compounds may exhibit versatile physical properties and support the evaluation of its possible applications in novel devices. However, very few efforts have been made to integrate them in a heterostructure and thereby exploit their complimentary functionalities. The integration of perovskite manganite and wurtzite ZnO in a heterostructure remains challenging because they have different crystal structures. ZnO has been adopted as a buffer layer in perovskite oxide capacitors [10]. The manganite/ZnO thin-film heterostructures were recently found to exhibit excellent rectifying behavior over a particular temperature range [11,12]. However, the details of the structural information of perovskite/wurtzite oxide thin-film heterostructures on perovskite single-crystal substrates are lacking. In this work, the perovskite manganite/ZnO thin-film heterostructures were synthesized by sputtering. The growth and characterization of the heterostructures were shown in this work.

* Tel.: +886 2 24622192; fax: +886 2 24625324.
E-mail address: yuanvictory@gmail.com.

0272-8842/$36.00
doi:10.1016/j.ceramint.2010.10.028

2. Experiments

The ZnO/$SrTiO_3$ (STO) and the $(La_{0.7}Sr_{0.3})MnO_3$ (LSMO)/ZnO/STO samples were fabricated by radio-frequency magnetron sputtering. Single-crystal STO with (1 0 0)-orientation was used as substrates. STO substrates were cleaned with acetone and methanol. The substrates were then post-annealed in O_2 atmosphere for 1 h to obtain ultra-smooth surface structure. ZnO ceramic target with a purity of 99.99% was adopted to grow ZnO thin films. LSMO target with Sr content of 0.3 was used to grow LSMO thin films on the ZnO/STO substrates. The ZnO film thickness is fixed at around 200 nm. The thickness of LSMO thin films was varied from 60 to 180 nm. During ZnO thin film deposition, the substrate temperature was varied from 400 to 700 °C. The deposition temperature of LSMO thin films was fixed at 700 °C. The pressure of working gas during deposition of the ZnO and LSMO thin films was fixed at 15 mTorr with an Ar/O_2 ratio of 3:2.

The crystallographic structures of the heterostructures were analyzed by measurements of high resolution X-ray diffraction (XRD). The surface morphology of the heterostructures was examined with an atomic force microscopy (AFM). The room temperature dependent photoluminescence (PL) spectra are obtained using the 325 nm line of a He-Cd laser. A superconducting quantum-interference device magnetometer was used to measure the magnetization of the LSMO/ZnO/STO samples.

3. Results and discussion

Fig. 1(a) exhibits the XRD patterns of the 200 nm-thick ZnO thin films grown on the STO substrates at various temperatures. The XRD patterns include well-defined (1 1 0) Bragg peaks from the ZnO thin films. The intensity of the (1 1 0) Bragg peak increases with growth temperature. The XRD patterns reveal that ZnO/STO thin films are highly (1 1 0)-oriented when the growth temperature is above 600 °C. Fig. 1(b) shows texture coefficient of the ZnO/STO thin films grown at various temperatures. The texture coefficient is defined as the intensity ratio $I(1\,1\,0)/[I(0\,0\,2) + I(1\,1\,0)]$ of the ZnO Bragg reflections. The background intensity of diffraction peaks was deducted before the calculation. The texture coefficient of the ZnO/STO thin film that was grown at the lowest temperature considered herein, 400 °C, is 57.7%. The higher growth temperature, 600 °C, is clearly associated with an enhancement of the appearance of preferred-(1 1 0) crystallographic plane in the ZnO/STO thin film. The texture coefficient attains 96.8% at a growth temperature of 600 °C. The ZnO/STO thin film that was grown at 700 °C has a perfect (1 1 0) crystallographic feature. The XRD results show that a preferred-(1 1 0) ZnO/STO thin film can only be grown at a sufficiently high substrate temperature. A ZnO thin film with a preferred-(1 1 0) orientation has also been grown by sputtering deposition on STO at a high temperature [13].

Fig. 2 plots the full widths at half maxima (FWHM) of ZnO(1 1 0) Bragg reflections from the ZnO/STO thin films that were grown at 600 and 700 °C. The FWHM value of ZnO(1 1 0) Bragg reflection for the film that was grown at 600 °C is ∼0.8° and that of the film grown at 700 °C is 0.54°. A high growth temperature enhances not only the (1 1 0)-textured feature of the ZnO/STO thin film but also its crystalline quality.

Fig. 3 shows the PL spectra of the ZnO/STO thin films grown at various temperatures. The relative intensity of the dominant peak at ∼381 nm increased with growth temperature because a highly crystalline ZnO/STO thin film was formed at a high temperature. The relationship between the PL spectra and the growth temperature of the ZnO/STO thin film is consistent with the XRD results. Moreover, the ZnO/STO thin films grown at low growth temperatures exhibit dominant visible emission, because they are of moderate crystalline quality. A low growth temperature may result in a high density of defects in a ZnO/STO thin film. The large variations in the UV and visible emission energies with growth temperature may explain the origin of defects and crystalline quality of such thin films. According to explanations presented in previous works [14,15], the quality of ZnO strongly influences the PL intensity ratio between the UV and visible emissions. The UV-to-visible emission ratio increases with growth temperature (Fig. 4). The UV-to-visible ratio of the ZnO/STO thin film grown at 700 °C is around 8.8. The increase in the ratio with growth temperature may be associated with a decrease in the number of point defects. These results show that a high-quality (1 1 0)-oriented ZnO thin film that emits UV light at room temperature can be formed on the STO substrate.

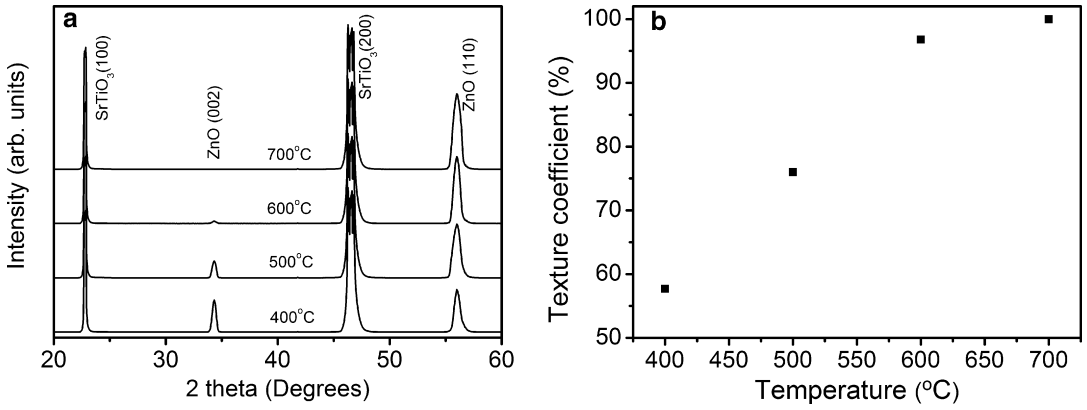

Fig. 1. (a) XRD patterns of ZnO/STO thin films grown at various temperatures. (b) Texture coefficient of ZnO/STO thin films grown at various temperatures.

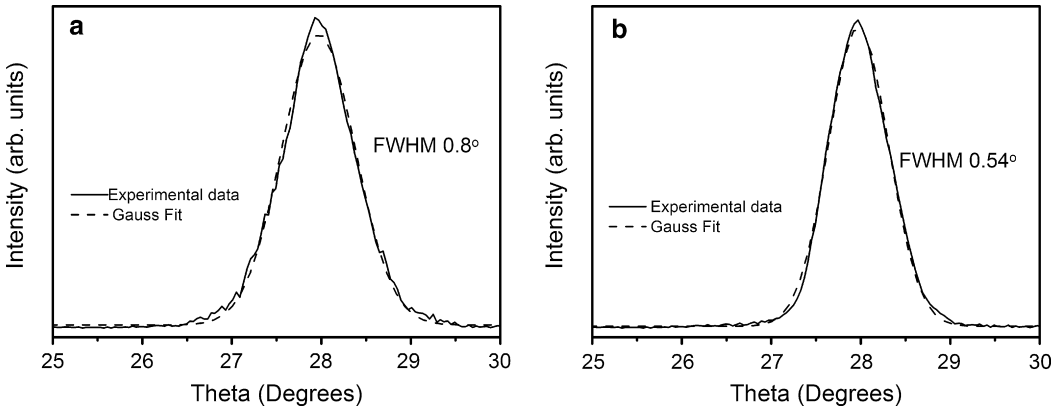

Fig. 2. Rocking curves of the (1 1 0) Bragg reflection of ZnO thin films grown at various temperatures. (a) 600 °C and (b) 700 °C.

Fig. 5 shows the XRD patterns of the LSMO/ZnO/STO heterostructures with various LSMO thicknesses. The XRD patterns include Bragg peaks that correspond to the (1 1 0) Bragg reflection of ZnO, and the (0 0 1), (1 1 0) and (0 0 2) Bragg reflections of LSMO, suggesting that LSMO films are polycrystalline on the ZnO(1 1 0)/STO(1 0 0). A thicker LSMO film has a stronger (0 0 *l*)-preferred orientation than that of the thinner one. Additionally, the peak position of the Bragg reflections of the LSMO thin film increases with film thickness. According to Fig. 5, the (0 0 *l*) Bragg reflections of the LSMO thin films with a thickness of <180 nm are to the left of the (*h* 0 0) Bragg reflections of the STO substrate. The out-of-plane lattice constant of a 180 nm-thick LSMO thin film is determined to be ∼0.387 nm which agrees closely with the bulk value [5,16]. The lattice constant of the 60 nm-thick LSMO is ∼0.399 nm. Fig. 6 plots thickness-dependence of lattice distortion of various LSMO thin films. The lattice distortion is defined as $(a_{exp} - a_{buk})/a_{buk}$, where a_{exp} is the lattice constant calculated from the (0 0 2) Bragg reflection of LSMO thin films and a_{buk} is the lattice constant (0.387 nm) of bulk LSMO. The lattice distortion decreases as the film thickness increases and the 180 nm-thick LSMO film does not exhibit distinct lattice distortion. Decreasing lattice distortion with increasing film thickness has also been identified for

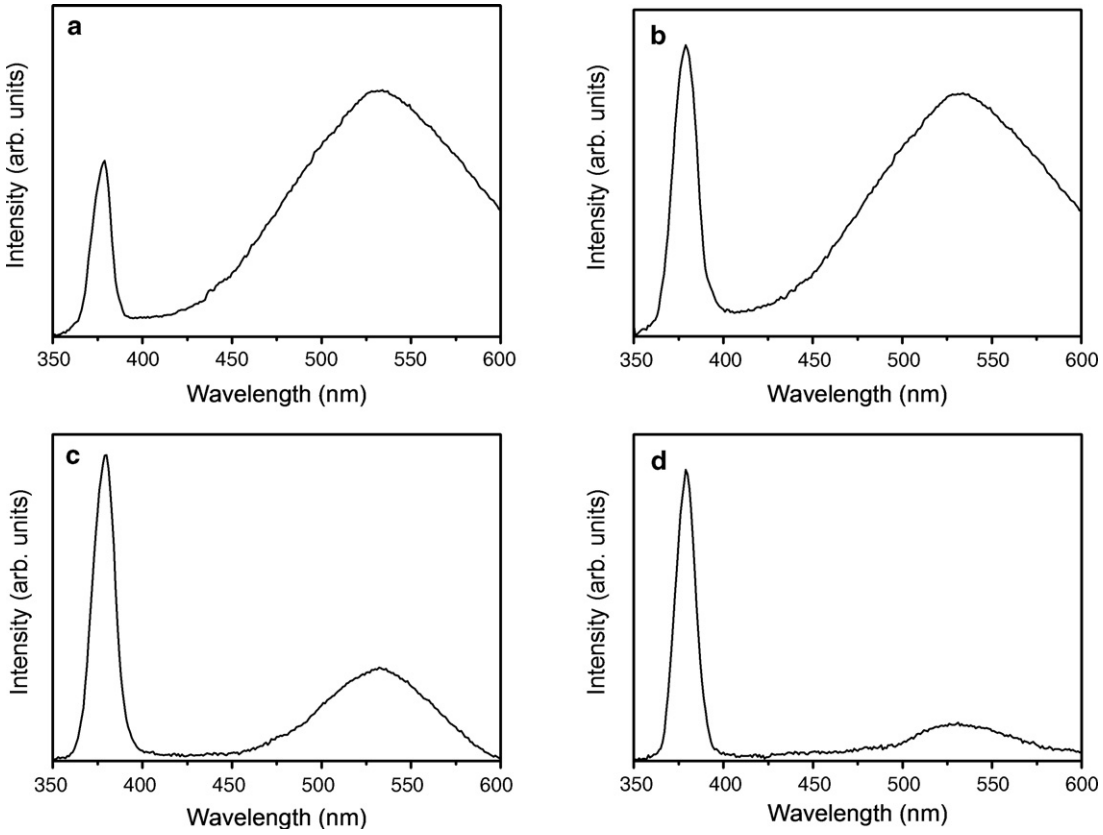

Fig. 3. PL spectra of ZnO/STO thin films grown at various temperatures. (a)400 °C, (b)500 °C, (c)600 °C, and (d) 700 °C.

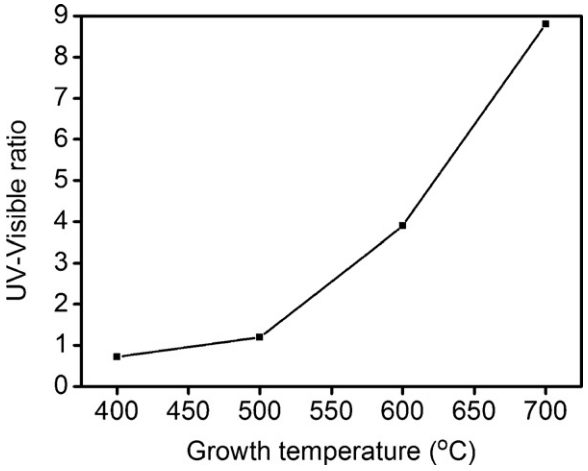

Fig. 4. UV–visible ratio of PL spectra for ZnO/STO thin films grown at various temperatures.

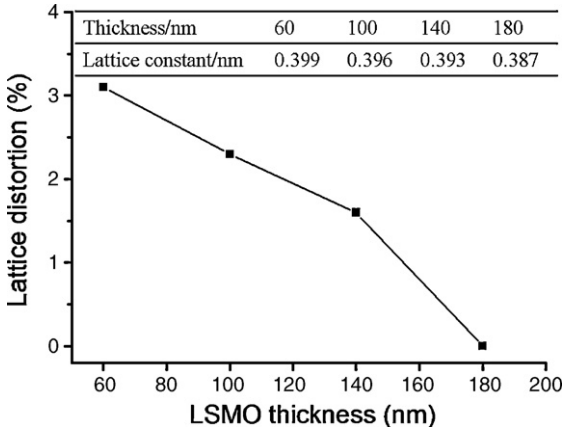

Fig. 6. The size of lattice distortion of LSMO thin films with various thicknesses. The lattice parameters of LSMO thin films with various thicknesses are shown in the inset.

sputtered oxide thin films [17], perhaps because longer sputtering produces a denser film [18].

Fig. 7 depicts the evolution of surface roughness as a function of LSMO thickness. The surface roughness of an LSMO film steadily increases with its thickness. The AFM images in Fig. 7 show the surface features of LSMO thin films with thicknesses of 60 and 180 nm. The AFM image of a 60 nm-thick LSMO thin film presents small three-dimensional islands on its surface. The thick LSMO film has relatively large surface grains. The grain size in sputtered perovskite oxide thin films increased with thickness [19]. Minimization of surface energy is believed to drive the coalescence of three-dimensional islands [20]. The increase in the grain size with film thickness further roughens the surface roughness of LSMO thin films.

A superconducting quantum interference device magnetometer was used to measure the magnetization of the samples. The magnetization vs. temperature (M–T) curves of the LSMO/ZnO/STO heterostructure films are shown in Fig. 8(a). All the M–T curves show a ferromagnetic-paramagnetic transition. The Curie temperatures (T_c) of the LSMO/ZnO/STO heterostructure films were evaluated from curves of magnetization vs. temperature. The T_c values of LSMO/ZnO/STO films with LSMO thicknesses of 60, 100, 140 and 180 nm are around 122, 195, 260 and 298 K, respectively. Lattice distortion in the heterostructure reportedly significantly reduces the T_c of manganite oxides [21]. Furthermore, some theoretical calculations and experimental works involving the effect of both orbital stability and Mn–O bond length confirmed that lattice distortion is an important factor in affecting magnetic properties of manganites [22]. LSMO with less lattice distortion and better crystalline quality has a higher T_c. Although a 180 nm-thick LSMO thin film exhibits no measurable lattice distortion, the T_c of 180 nm-thick LSMO is below that for the bulk material (~355 K) herein. The relatively low T_c of the 180 nm-thick LSMO thin film may follow from the fact that the quality of bulk material is typically better than that of the corresponding thin-film material. Another factor that may be responsible for the relatively low T_c of an LSMO film with the bulk lattice constant in the heterostructure is imperfection at the ZnO/LSMO interface. LSMO and ZnO

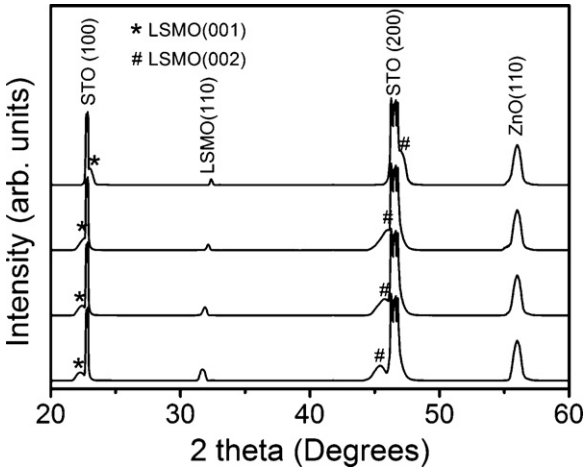

Fig. 5. XRD patterns of LSMO/ZnO/STO heterostructures with various LSMO thicknesses. The LSMO film thickness for the XRD patterns from top to bottom is 180 to 60 nm.

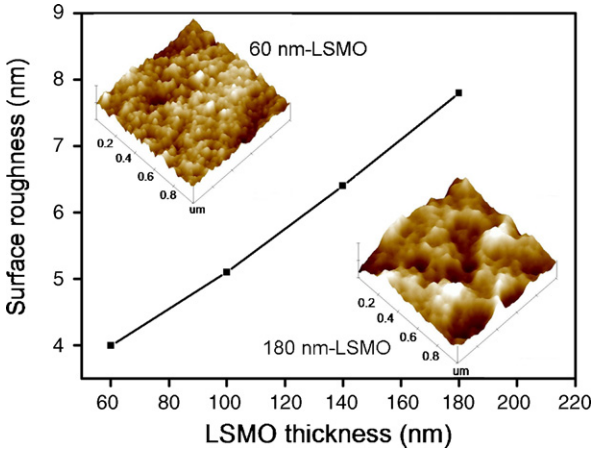

Fig. 7. Surface roughness vs. LSMO thickness for LSMO/ZnO/STO heterostructures. The AFM images of 60 and 180 nm-thick LSMO films are shown in the insets.

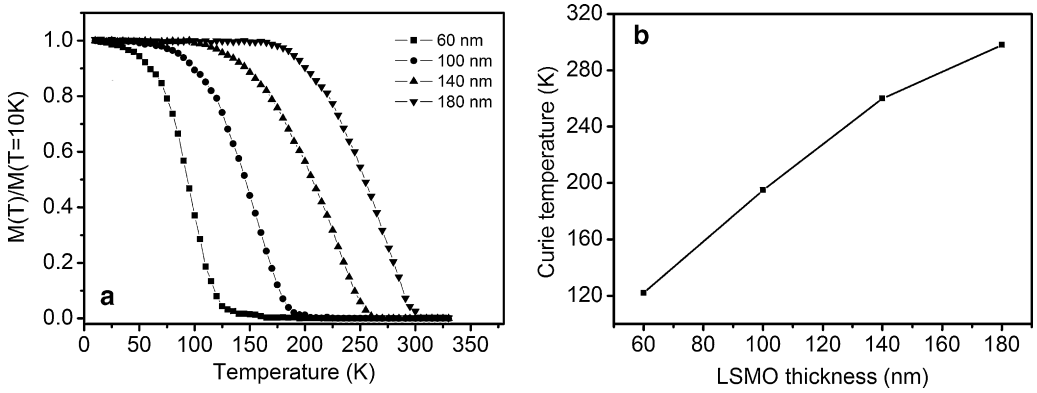

Fig. 8. (a) Normalized magnetization vs. temperature curves for LSMO/ZnO/STO heterostructures. The data were obtained in a field of 0.7 T. (b) Curie temperature of heterostructures with various LSMO thicknesses.

generally exhibit different types of conductivity [11]. The construction of an LSMO/ZnO heterostructure may degrade LSMO/ZnO interface feature. The imperfection of the heterointerface may further degrade the magnetic properties of the heterostructures. The results of magnetization vs. temperature herein show that the physical properties of the LSMO can be modulated by engineering the heterostructure. This fact may open up a new approach to designing LSMO-based oxides for use in devices in the future.

4. Conclusions

ZnO/STO thin films with a highly preferred (1 1 0)-orientation can be grown at a temperature higher than 600 °C. A high growth temperature enhances not only the (1 1 0)-textured feature of the ZnO/STO thin film but also its crystalline quality. Moreover, the PL results show that the (1 1 0)-oriented ZnO thin films emits UV light at room temperature. The LSMO thin films grown on ZnO(1 1 0)/STO(1 0 0) are polycrystalline. A thicker LSMO film exhibits a stronger (0 0 *l*)-preferred orientation, a greater surface roughness and less lattice distortion. The M–T results demonstrate crystalline quality and lattice distortion affect the magnetic properties of the LSMO thin films and that the physical properties of manganite thin films can be modulated by the formation of a heterostructure with ZnO.

Acknowledgements

This work was financially supported by the National Science Council of the Republic of China (Grant Nos. NSC 98-2911-I-270-001-2 and NSC 99-2221-E-019-055) and the National Taiwan Ocean University (Grant No. NTOU-RD-AA-2010-104031).

References

[1] G.J. Snyder, R. Hiskes, S. DiCarolis, M.R. Beasley, T.H. Geballe, Intrinsic electrical transport and magnetic properties of $La_{0.67}Ca_{0.33}MnO_3$ and $La_{0.67}Sr_{0.33}MnO_3$ MOCVD thin films and bulk material, Phys. Rev. B 53 (1996) 14434–14444.

[2] Y.C. Liang, Y.C. Liang, Quantifying strain effects on physical properties of $La_{0.68}Ba_{0.32}MnO_3$ epilayers and heterostructures, J. Electrochem. Soc. 154 (2007) P147–P151.

[3] J.Z. Sun, W.J. Gallagher, P.R. Duncombe, L. Krusin-Elbaum, R.A. Altman, A. Gupta, Y. Lu, G.Q. Gong, G. Xiao, Observation of large low-field magnetoresistance in trilayer perpendicular transport devices made using doped manganate perovskites, Appl. Phys. Lett. 69 (1996) 3266–3268.

[4] Y.C. Liang, Y.C. Liang, Correlation between lattice modulation and physical properties of $La_{0.72}Ca_{0.28}MnO_3$ films grown on $LaAlO_3$ substrates, J. Crystal Growth 303 (2007) 638–644.

[5] Y.C. Liang, Y.C. Liang, Strain-dependent surface evolution and magneto-transport properties of $La_{0.7}Sr_{0.3}MnO_3$ epilayers on $SrTiO_3$ substrates, J. Crystal Growth 304 (2007) 275–280.

[6] Y.C. Liang, Growth-temperature-dependent microstructure and ferromagnetic properties of perovskite manganite-based heterostructures, Ceram. Int. 36 (2010) 2359.

[7] Y.C. Liang, H.Y. Lee, Y.C. Liang, H.J. Liu, K.F. Wu, T.B. Wu, Physical properties of strained artificial superlattices of $(La_{0.7}Ba_{0.3})MnO_3/LaNiO_3$, J. Electrochem. Soc. 153 (2006) J117–J121.

[8] D.M. Bagnall, Y.F. Chen, Z. Zhu, T. Yao, M.Y. Shen, T. Goto, High temperature excitonic stimulated emission from ZnO epitaxial layers, Appl. Phys. Lett. 73 (1998) 1038–1040.

[9] S.F. Yu, C. Yuen, S.P. Lau, H.W. Lee, Zinc oxide thin-film random lasers on silicon substrate, Appl. Phys. Lett. 84 (2004) 3244–3246.

[10] X.S. Wang, Y.J. Wang, J. Yin, Z.G. Liu, Enhanced ferroelectric properties of $Pb(Zr_{0.52}Ti_{0.48})O_3$ films on $Pt/TiO_2/SiO_2/Si(0\,0\,1)$ using ZnO buffer layer, Scripta Mater. 46 (2002) 783–787.

[11] K. Lord, D. Hunter, T.M. Williams, A.K. Pradhan, Photocarrier injection effect and *p–n* junction characteristics of $La_{0.7}Sr_{0.3}MnO_3$/ZnO and Si heterostructures, Appl. Phys. Lett. 89 (2006) 052116–052118.

[12] K.X. Jin, S.G. Zhao, C.L. Chen, J.Y. Wang, B.C. Luo, Positive colossal magnetoresistance effect in $ZnO/La_{0.7}Sr_{0.3}MnO_3$ heterostructure, Appl. Phys. Lett. 92 (2008) 112512–112514.

[13] Y.C. Liang, Growth and characterization of nonpolar *a*-plane ZnO films on perovskite oxides with thin homointerlayer, J. Alloy Compd. 508 (2010) 158–161.

[14] B. Cao, F. Sun, W. Cai, Electrochem. Electrodeposition-induced highly oriented zinc oxide ordered pore arrays and their ultraviolet emissions, Solid-State Lett. 8 (2005) G237–G240.

[15] P.T. Hsieh, Y.C. Chen, K.S. Kao, C.M. Wang, Luminescence mechanism of ZnO thin film investigated by XPS measurement, Appl. Phys. A 90 (2008) 317–321.

[16] A. Tiwari, A. Chugh, C. Jin, D. Kumar, J. Narayan, Integration of single crystal $La_{0.7}Sr_{0.3}MnO_3$ films with $Si(0\,0\,1)$, Solid State Commun. 121 (2002) 679–682.

[17] Y. Shigesato, S. Takaki, T. Haranou, Crystallinity and electrical properties of tin-doped indium oxide films deposited by DC magnetron sputtering, Appl. Surf. Sci. 48–49 (1991) 269–275.

[18] Z.W. Yang, S.H. Han, T.L. Yang, L. Ye, D.H. Zhang, H.L. Ma, C.F. Cheng, Bias voltage dependence of properties for depositing transparent conducting ITO films on flexible substrate, Thin Solid Films 366 (2000) 4–7.
[19] Y.C. Liang, Thickness dependence of structural and electrical properties of electric field tunable $Ba_{0.6}Sr_{0.4}TiO_3$ transparent capacitors, Electrochem. Solid-State Lett. 12 (2009) G54–G56.
[20] N. Wakiya, K. Kuroyanagi, Y. Xuan, K. Shinozaki, N. Mizutani, Nucleation and growth behavior of epitaxial $Pb(Zr,Ti)O_3$/MgO(1 0 0) observed by atomic force microscopy, Thin Solid Films 357 (1999) 166–172.
[21] Y. Lu, J. Klein, C. Hofener, B. Wiedenhorst, J.B. Philipp, F. Herbstritt, A. Marx, L. Alff, R. Gross, Magnetoresistance of coherently strained $La_{2/3}Ba_{1/3}MnO_3/SrTiO_3$ superlattices, Phys. Rev. B 62 (2000) 15806–15814.
[22] F.S. Razavi, G. Gross, H.-U. Habermeier, O. Lebedev, S. Amelinckx, G. Van Tendeloo, A. Vigliante, Epitaxial strain induced metal insulator transition in $La_{0.9}Sr_{0.1}MnO_3$ and $La_{0.88}Sr_{0.1}MnO_3$ thin films, Appl. Phys. Lett. 76 (2000) 155–158.